Computers and Geotechnics 36 (2009) 493–502

Contents lists available at ScienceDirect

Computers and Geotechnics

journal homepage: www.elsevier.com/locate/compgeo

Drained bearing response of shallow foundations on structured soils

D.S. Liyanapathirana [a,*], J.P. Carter [b], D.W. Airey [c]

[a] Department of Civil, Mining and Environmental Engineering, University of Wollongong, Northfields Avenue, Wollongong, NSW 2522, Australia
[b] Faculty of Engineering and Built Environmental, The University of Newcastle, Callaghan, NSW 2308, Australia
[c] Department of Civil Engineering, University of Sydney, NSW 2006, Australia

ARTICLE INFO

Article history:
Received 3 May 2007
Received in revised form 22 April 2008
Accepted 23 April 2008
Available online 11 June 2008

Keywords:
Structured soil
Shallow foundations
Bearing capacity
Structured Cam Clay model
Finite element method

ABSTRACT

This paper examines the drained bearing response of circular footings resting on structured soil deposits. Numerical simulations have been carried out using a finite element formulation of the Structured Cam Clay model. A parametric study was conducted by varying the parameters that govern the behaviour of structured soils and guidelines are given for designers to identify when effects of the soil structure are important. Under fully drained conditions, deformation within the structured soil supporting the footing usually occurs as a local or punching shear failure due to high compressibility of the structured soil and the mobilised bearing pressure increases with the footing movement, without reaching an ultimate value. A novel approximate method is presented to obtain the load–displacement response of a rigid circular footing resting on the surface of a structured soil deposit. This requires the properties of the soil in the reconstituted state and two additional parameters, which govern the natural structure of the soil. The proposed method has been applied to a published case study, where plate load test results are given for rigid circular steel plates resting on structured soil deposits. Fair agreement is observed between the computed and experimental results, suggesting the approximate method may be useful in design studies of foundations on structured soil deposits.

1. Introduction

Accurate assessment of the bearing resistance of the ground is an important step in the process of evaluating the stability and economy of structures. Although most structures are founded on footings resting on natural soil deposits having a structure, relatively little is known about the influence of soil structure on the bearing response of these footings. In classical bearing capacity theories (e.g., [17]) and cavity expansion theories (e.g., [7,18,2]), which are commonly used by practising geotechnical engineers to assess foundation capacity, the influence of soil structure on the bearing capacity is not directly taken into account. The main objective of this paper is therefore to examine the significance of soil structure on the long-term (fully drained) bearing resistance of circular footings resting on the surface of structured soil deposits.

Generally, structured soils behave differently from the same material in a reconstituted state. Although soil structure may arise from many different causes, its effects on the mechanical behaviour have been shown to be similar [8]. Various geological processes can cause a loss of soil structure either by inducing yield (damaging the bonding or permanently rearranging the particles) or by removing bonding agents. Significant difficulties have been encountered in cases where the structural features of the soil dominate its engineering behaviour. The low driving resistance of piles observed in carbonate soils at the North Rankin offshore gas production platform, Australia [6] and the subsidence induced during hydrocarbon extraction from reservoirs at Ekofisk, North Sea [11] are but two examples.

Recently, there have been important developments in understanding of the mechanics of structured soils. At a fundamental level, there have been useful advances in formulating constitutive models incorporating the influence of soil structure, such as those proposed by Gens and Nova [4], Whittle [19], Rouainia and Muir Wood [15], and Liu and Carter [9]. In this paper, the constitutive model for structured soils proposed by Liu and Carter [9] has been applied to study the long-term (fully drained) bearing response of surface circular footings resting on structured soils. Numerical simulations were carried out by incorporating the Structured Cam Clay model in the finite element program AFENA [1] developed at the University of Sydney. The finite element formulation of this constitutive model can be found in Liyanapathirana et al. [10]. The influence of soil structure on the predicted load–displacement response has been investigated for a range of model parameters, which govern the structural features of the soil. Guidelines are provided to identify the level of significance of the soil structure on the bearing response, and a method is presented to obtain approximately the

* Corresponding author. Tel.: +61 2 4221 3035.
E-mail address: saml@uow.edu.au (D.S. Liyanapathirana).

0266-352X/$ - see front matter © 2008 Elsevier Ltd. All rights reserved.
doi:10.1016/j.compgeo.2008.04.004

fully drained load–displacement response of a surface circular footing resting on a structured soil deposit. This method requires knowledge of the reconstituted soil parameters and two additional parameters that describe the structure of the natural soil.

2. Parameters defining soil structure

In the Structured Cam Clay model [9] four additional parameters are used to introduce the structural features of the soil into the Modified Cam Clay model developed originally by Roscoe and Burland [14]. The destructuring index, b, defines the rate at which the soil structure is lost during the process of destructuration. The size of the initial yield surface, p'_{co}, (see Fig. 1) defines the mean effective stress at which yielding or the destructuration of the structured soil begins. The additional voids ratio sustained by the structured soil at the time of commencement of yielding is Δe_i and the influence of soil structure on the plastic potential is described by another parameter, ω. These parameters can be determined directly from an isotropic compression test on an intact (undisturbed) soil specimen [9].

The yield surface of the Structured Cam Clay model in $p' - q$ space is elliptical and passes through the origin of the stress space, similar to the Modified Cam Clay model, but non-associated plastic flow is assumed. In what follows, all (intrinsic) properties of the same soil at the reconstituted state are denoted by the superscript $*$.

3. Finite element model

The axisymmetric finite element model used for the analysis of circular footings resting on structured soil consists of 15-node triangular elements and extends 7.5B in radial and vertical directions as shown in Fig. 2, where B is the radius of the circular footing. For all cases presented, a smooth contact between the base of the footing and the soil is assumed and this will be discussed in Section 4.

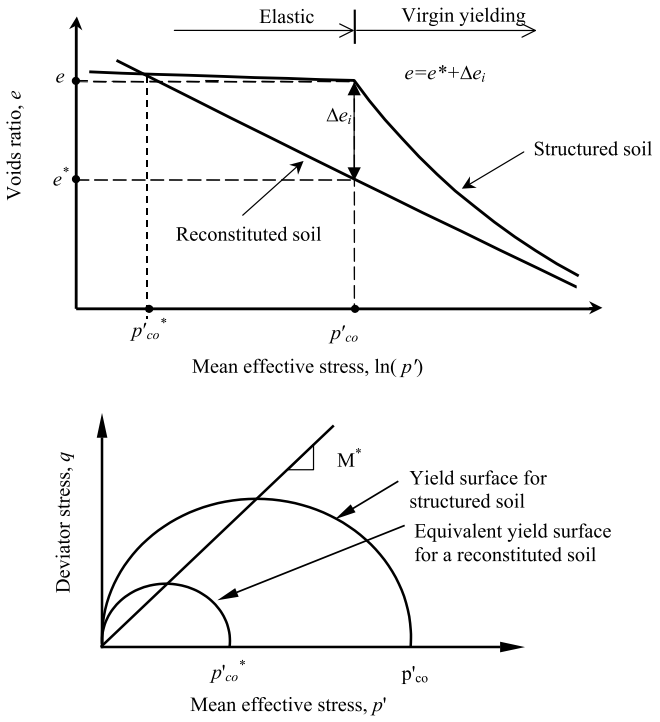

Fig. 1. Idealisation of the compression and yield behaviour adopted in the Structured Cam Clay model.

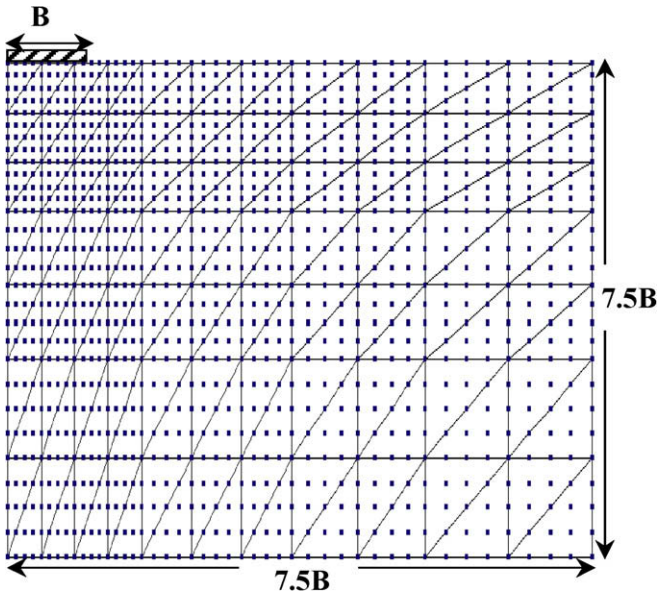

Fig. 2. Finite element mesh with 15-node triangular elements used for the analysis.

The water table is assumed to be at the ground surface. The bottom boundary is restrained against vertical and horizontal movement. The left and right hand side boundaries of the mesh were restrained against horizontal movement. Footing is pushed into the ground controlling the displacement increments. The size of the increments used in the elastic and plastic regions shown in Fig. 3a are 0.001 m ($d\delta/B = 0.0002$) and 0.0005 m ($d\delta/B = 0.0001$), respectively, and the analysis is carried out as a small strain finite element analysis. Details of the incremental solution scheme are not described here as it can be found in the AFENA manual [1].

4. Mode of bearing failure

The bearing capacity of a footing is often mobilised as a shear failure that occurs within the soil supporting the footing. It is generally recognized that there are three principal modes of shear failure: general shear failure, local shear failure and punching shear failure. Numerical analyses have been carried out to investigate the possible modes of failure for structured soils. Fig. 3a shows a normalized plot of the mobilized bearing pressure against the footing settlement for a 5 m diameter rigid circular footing resting on a structured soil deposit, where q_{av} is the average applied footing pressure, p'^{*}_{co} is mean effective stress at which yielding of the reconstituted soil begins, as shown in Fig. 1, δ is the footing settlement and B is the footing diameter. The specific details for this fairly typical case are shown in Table 1. No visible collapse is observed and a

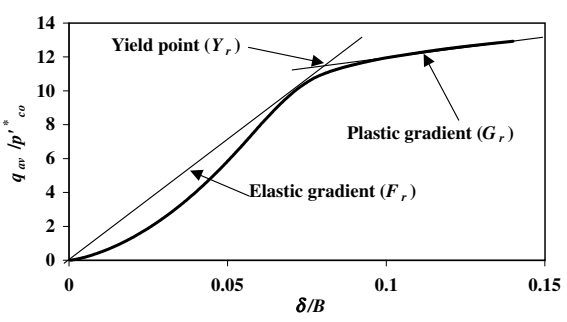

Fig. 3a. Bearing pressure mobilisation with footing movement.

Table 1
Properties of structured soil assumed for typical example

Symbol	Description	Value
Reconstituted soil properties		
λ^*	Gradient of the normal compression line in $e - \ln(p')$ space	0.16
κ^*	Gradient of the unloading and reloading line in $e - \ln(p')$ space	0.06
M^*	Aspect ratio for the yield surface	1.2
ν^*	Poisson's ratio	0.25
e^*_{cs}	Void ratio at the $p' = 1$ on the CSL in $e - \ln(p')$ space	1.8
dp'^*_{co}/dz	Gradient of p'^*_{co} with depth below the ground surface	10 kPa/m
p'^*_{co}	Size of the initial yield surface for the structured soil at ground surface	20.0 kPa
K_o	Coefficient of earth pressure at rest	0.6
γ	Bulk unit weight of soil (water table assumed at ground surface)	20 kN/m^3
Additional parameters defining soil structure		
b	Destructuring index	0.25
Δe_i	Additional voids ratio sustained by soil structure	0.25
p'_{co}	Size of the initial (structural) yield surface at ground surface	243.65 kPa
ω	Parameter defining the plastic potential	1

continuous increase in vertical load is needed to maintain the footing movement in the downward direction. Fig. 3b shows the cumulative displacement vectors at a displacement of 10% relative to the diameter of the footing. The displacement vectors are predominantly in the vertically downward direction. Although a few vectors are at an angle to the vertical, they do not show a flow pattern in a radial shearing zone. Therefore, it can be concluded that the deformation of the structured soil beneath the footing occurs predominantly as a punching shear failure in this case. The load–displacement response observed for calcarenite by Sharp and Seters [16], calcareous sand by Poulos et al. [13] and Poulos and Chua [12], artificially cemented calcareous sand by Yeoh [21] and carbonate sands by Islam [5] are consistent with the finite element results obtained by considering different parameter sets of structures soils, where the applied load continuously increase with the movement of the footing. This behaviour is typically observed in foundations resting on compressible soils, where failure occurs predominantly as a punching or local shear failure.

Results obtained for smooth and rough contact conditions at the footing–soil interface are nearly the same when the failure occurs as punching or local shear failure because at the footing–soil interface, soil deformation is predominantly in the vertical direction. Therefore in what follows, a smooth contact is assumed at the footing–soil interface.

5. Prediction of bearing response curve

Since failure of the soil beneath the footing occurs as a punching or local shear, the mobilised bearing pressure continuously increases with the footing movement, apparently without reaching an ultimate bearing capacity, at least within the bounds of a small displacement approach. For punching shear, the bearing pressure mobilized at a displacement of 10% of the footing diameter is often defined as the "bearing capacity" [18] (Poulos and Chua, [12]). However, this is an arbitrary value. Sharp and Seters [16] and Islam [5] showed that for punching or local shear, bearing pressure curves can be approximated by bilinear relationships. Although both sections of the curve involve elasto-plastic behaviour, the first section of the curve represents predominantly elastic penetration of the footing and the second represents predominantly plastic penetration of the footing. Therefore the first section of the curve is termed as 'elastic' and the second section is termed as 'plastic'. If gradients of the elastic (F_r) and plastic (G_r) parts and the yield point (Y_r), as shown in Fig. 3a, are known, an approximate curve of dimensionless bearing pressure (q_{av}/p'^*_{co}) versus dimensionless displacement (δ/B) can be predicted. Hence, the bearing pressure can be obtained for any vertical movement of the footing, instead of assigning an arbitrary value as the ultimate bearing capacity.

In the following sections, a simple method is outlined to obtain the long-term (fully drained) bearing response of circular footings resting on structured soil deposits that has been developed from the results of numerical analyses using the Structured Cam Clay model. The value of p'^*_{co} used in the finite element analyses is varied along the depth of the soil deposit as given in Table 1 to simulate an overconsolidated state within the soil deposit below the footing because in normally consolidated state, soil does not possess any structure. Hence the dimensionless parameter q_{av}/p'^*_{co} is calculated based on the p'^*_{co} at the base level of the footing. First the bearing response is predicted for the soil in a reconstituted state, neglecting the structural properties of the soil. Further analyses incorporating the structural properties of the soil are then used to

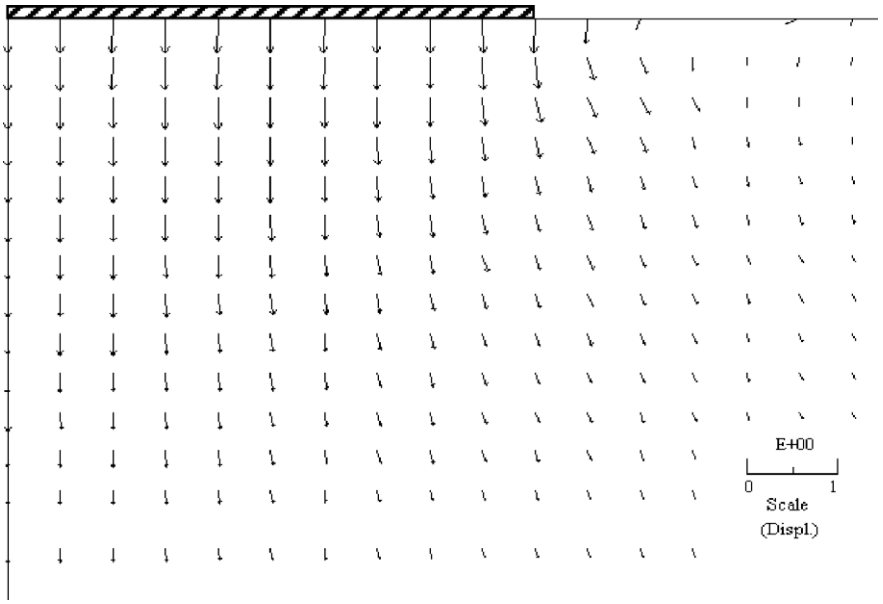

Fig. 3b. Cumulative displacement vectors beneath the footing at a displacement of 0.1B (drained).

modify the response of the reconstituted soil and obtain the bearing response for the structured soil.

5.1. Bearing response curve for reconstituted soil ($\Delta e_i = 0$)

Here the properties of the soil are defined in terms of the critical state soil parameters: the gradient of the normal compression line in the $e - \ln(p')$ space, λ^*, the gradient of the unloading and reloading line in $e - \ln(p')$ space, κ^*, the aspect ratio of the yield surface, M^*, Poisson's ratio, v^*, and the value of voids ratio at a mean effective stress of 1 kPa on the critical state line in $e - \ln(p')$ space, e^*_{cs}.

For reconstituted soils, it was found that for a unique value of the combined parameter $\gamma' B/p'^*_{co}$, where γ' is the effective unit weight of the soil, curves of the non-dimensional bearing pressure q_{av}/p'^*_{co} plotted against the non-dimensional footing settlement δB were almost the same, irrespective of the individual values of each variable. Islam [5] also demonstrated this result using a constitutive model developed specifically for carbonate sand.

When the additional voids ratio sustained by the structured soil at the time of first yielding, Δe_i, is zero, the Structured Cam Clay Model simulates reconstituted soil behaviour. Therefore, in this section, the influence of the reconstituted soil properties on the bearing response is studied using the Structured Cam Clay model with zero Δe_i. Each soil parameter defining intrinsic properties of the soil has been varied separately by keeping all other parameters equal to the values given in Table 1. Influence of Ko has not been considered here, as it does not significantly influence the bearing response. This has been observed by Woodward et al. [20] as well. For each parameter set, analysis was repeated for six different values of $\gamma' B/p'^*_{co}$ (viz., 0.76, 1.52, 2.28, 3.04, 3.8 and 4.75), which fall within the range of $\gamma' B/p'^*_{co}$ encountered in practice.

5.1.1. Influence of κ^* on bearing response

Fig. 4 shows the influence of κ^* on the bearing response for a 5 m diameter surface circular footing. The value of κ^* has been varied from 0.005 to 0.1. With a decrease in κ^*, the elastic gradient of the bearing response curve increases showing a stiffer response. The influence of κ^* on the yield point and the plastic gradient are not very significant, and they have been ignored for simplicity. To establish the proposed method for predicting the bearing capacity curve, only the influence of κ^* and $\gamma' B/p'^*_{co}$ on the elastic gradient has been considered.

Fig. 5 shows the variation of elastic gradient with κ^* and $\gamma' B/p'^*_{co}$. The influence of κ^* on the elastic gradient generally increases with increasing $\gamma' B/p'^*_{co}$. For $\kappa^* > 0.03$, the elastic gradient does not vary significantly with $\gamma' B/p'^*_{co}$. For the data points obtained from the finite element analyses shown in Fig. 5, the elastic gradient for the reconstituted soil, F_r, can be related to κ^* and $\gamma' B/p'^*_{co}$ as follows:

$$(F_r)_{\kappa^*} = 1.25(\kappa^*)^{-1}\left(\frac{\gamma' B}{p'^*_{co}}\right)^{0.6} \quad (1)$$

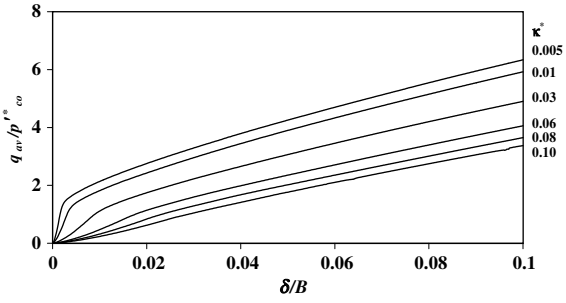

Fig. 4. Influence of κ^* on the bearing response ($B = 5$ m).

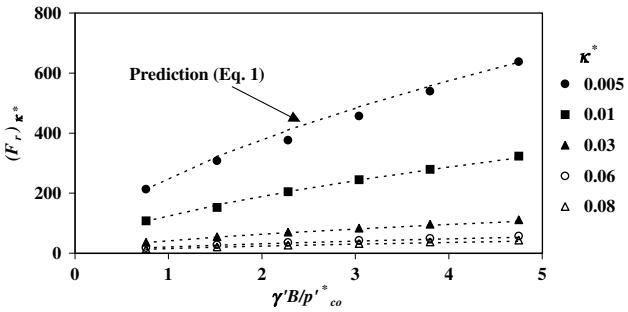

Fig. 5. Variation of elastic gradient, F_r, with κ^* and $\gamma' B/p'^*_{co}$.

5.1.2. Influence of λ^* on bearing response

Fig. 6 shows the bearing response for a 5 m diameter circular footing when λ^*, the plastic compressibility parameter for the soil, changes from 0.12 to 0.35. According to Fig. 6, the elastic gradient and the yield point are nearly the same for all values of λ^* considered in the analyses. However, beyond the yield point, the bearing pressure at a given settlement increases with decreasing λ^*. For example, when the footing displacement is 10% of the footing diameter, the bearing pressure obtained for $\lambda^* = 0.12$ is twice that obtained with $\lambda^* = 0.35$. Therefore, in the establishment of the proposed simplified method, only the influence of λ^* on the plastic gradient, G_r, has been taken into account.

Variation of the plastic gradient of the bearing response with $\gamma' B/p'^*_{co}$ for different values of λ^* is shown in Fig. 7. If $\gamma' B/p'^*_{co} \leqslant 1$, λ^* does not show any significant influence on the plastic gradient of the reconstituted soil, G_r. With an increase in $\gamma' B/p'^*_{co}$, the plastic gradient increases with decreasing λ^*. For example, when $\gamma' B/p'^*_{co} = 4.75$, the plastic gradient obtained with $\lambda^* = 0.12$ is three times that obtained with $\lambda^* = 0.35$. To sufficient accuracy the values of plastic gradient, G_r, obtained from the finite element predictions satisfy the following equation:

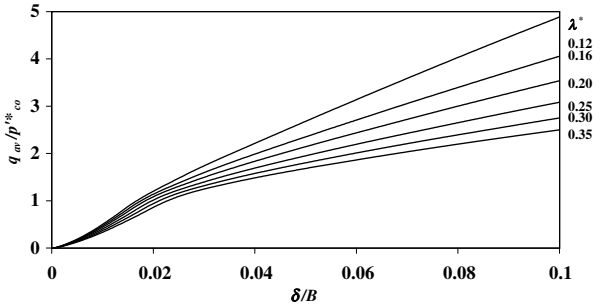

Fig. 6. Influence of λ^* on the bearing response ($B = 5$ m).

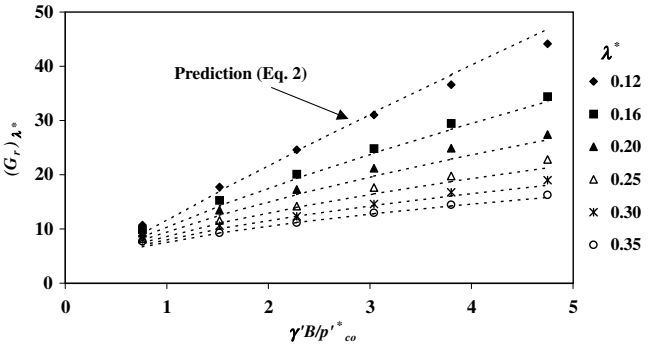

Fig. 7. Variation of plastic gradient, G_r, with λ^* and $\gamma' B/p'^*_{co}$.

$$(G_r)_{\lambda^*} = 5(\lambda^*)^{-0.4}\left(\frac{\gamma' B}{p'^*_{co}}\right)^n \quad (2)$$

where $n = 0.25(\lambda^*)^{-0.6}$.

5.1.3. Influence of M^* on bearing response

In the general bearing capacity equation proposed by Terzaghi [17], which is a widely used method to determine the bearing capacity of footings, the friction angle plays a major role in determining the drained or long-term bearing capacity. In the Structured Cam Clay model, M^*, which is the aspect ratio of the yield surface, is a function of the ultimate friction angle, φ'_{cs}, as shown below:

$$M^* = \frac{6\sin\phi'_{cs}}{3-\sin\phi'_{cs}} \quad (3)$$

Therefore, the influence of M^* on the bearing response reflects the influence of friction angle of the soil. Since the dependency of M^* on Lode's angle is not significant for axisymmetric problems, a constant M^* has been used in the analysis.

Fig. 8 shows the computed influence of M^* on the bearing response. The elastic gradient, F_r, which demonstrates predominantly the elastic penetration of the footing, does not depend on M^*. However, the yield point, Y_r, and the plastic gradient, G_r, which reflect the plastic penetration of the footing, change significantly with M^*.

Fig. 9 shows the combined influence of M^* and $\gamma' B/p'^*_{co}$ on the yield point. With an increase in M^*, the yield point increases showing a stiffer soil response. Also, for a particular value of M^*, the yield point increases with $\gamma' B/p'^*_{co}$. Based on the results obtained from the finite element analysis of footing response given in Fig. 9, the influence of M^* and $\gamma' B/p'^*_{co}$ on the yield point can be described to sufficient accuracy by:

$$(Y_r)_{M^*} = (M^*)^{1.25}\left(\frac{\gamma' B}{p'^*_{co}}\right)^m \quad (4)$$

where $m = 0.25(M^*)^{-0.75}$.

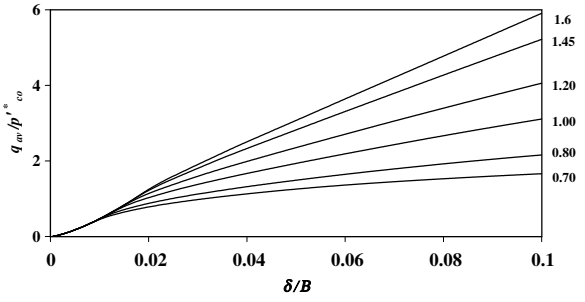

Fig. 8. Influence of M^* on the bearing response ($B = 5$ m).

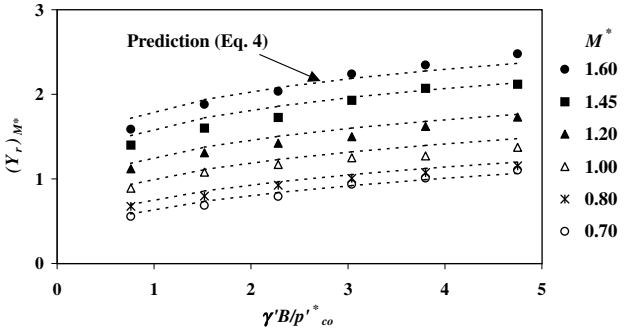

Fig. 9. Variation of yield point, Y_r, with M^* and $\gamma' B/p'^*_{co}$.

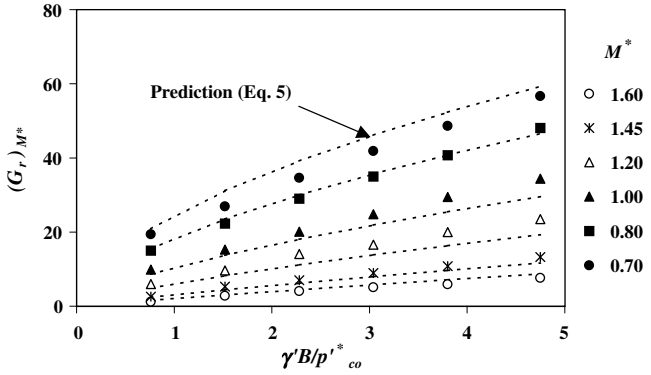

Fig. 10. Variation of plastic gradient, G_r, with M^* and $\gamma' B/p'^*_{co}$.

Fig. 10 shows the influence of M^* and $\gamma' B/p'^*_{co}$ on the plastic gradient, G_r. With an increase in M^*, the plastic gradient increases significantly. For example, there is a 7-fold increase in the plastic gradient when M^* increases from 0.7 to 1.6 for $\gamma' B/p'^*_{co} = 4.75$. The influence of M^* on the plastic gradient is more pronounced for larger values of $\gamma' B/p'^*_{co}$ than for smaller values of $\gamma' B/p'^*_{co}$. Based on the results obtained from the finite element analyses of the footing response given in Fig. 10, the combined influence of M^* and $\gamma' B/p'^*_{co}$ on the plastic gradient, G_r, can be represented by:

$$(G_r)_{M^*} = 6(M^*)^3\left(\frac{\gamma' B}{p'^*_{co}}\right)^l \quad (5)$$

where $l = 0.75(M^*)^{-0.6}$.

5.1.4. Influence of v^* on bearing response

In the Structured Cam Clay model, a constant value of Poisson's ratio, v^*, is usually assumed. Fig. 11 shows the influence of v^* on the bearing response for v^* varying from 0.1 to 0.4. For all values of v^*, the plastic gradient of the bearing response curve is nearly the same. Also the variation of yield point with v^* is not significant. Since the plastic gradient and yield point reflect predominantly plastic penetration of the footing, it can be concluded that the influence of Poisson's ratio is significant only during the elastic penetration. Therefore, in establishing the proposed simplified method for the assessment of bearing response of circular footings, the influence of v^* on both yield point, Y_r, and plastic gradient, G_r, has been ignored.

Fig. 12 shows the influence of v^* on the elastic gradient (F_r) for $\gamma' B/p'^*_{co}$ varying from 0.76 to 4.75. For $\gamma' B/p'^*_{co} \leqslant 1.0$, the influence of v^* on the elastic gradient is small compared to the larger values of $\gamma' B/p'^*_{co}$. Using the results given in Fig. 12, the influence of v^* and $\gamma' B/p'^*_{co}$ on elastic gradient, F_r, can be represented by:

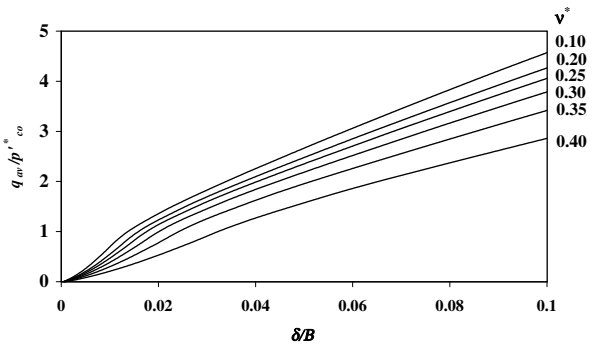

Fig. 11. Influence of v^* on the bearing response ($B = 5$ m).

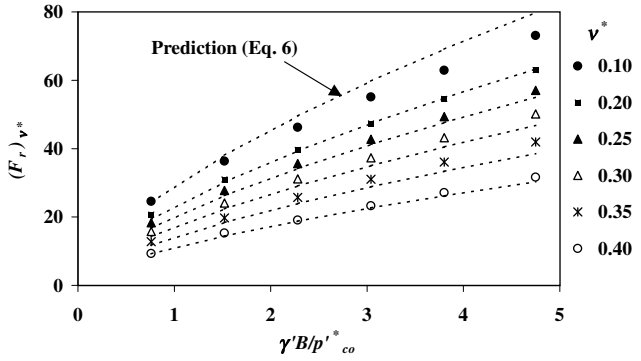

Fig. 12. Variation of elastic gradient, F_r, with v^* and $\gamma'B/p'^*_{co}$.

$$(F_r)_{v^*} = (35 - 60v^*)\left(\frac{\gamma'B}{p'^*_{co}}\right)^{0.6} \tag{6}$$

5.1.5. Influence of e^*_{cs} on bearing response

In this section, the influence of e^*_{cs} on the bearing response of a circular footing is investigated. Fig. 13 shows the bearing response for a 5 m diameter footing for e^*_{cs} varying from 1 to 3.2. With an increase in e^*_{cs}, the bearing resistance at a given footing displacement increases. For example, when e^*_{cs} increases from 1 to 3.2, the mobilized bearing resistance is doubled at a footing displacement of 10% relative to the diameter of the footing.

Both elastic and plastic gradients increase with increasing e^*_{cs}, but the influence of e^*_{cs} on the yield point is not significant. Figs. 14 and 15 show the influence of e^*_{cs} on the elastic and plastic gradients of the bearing response curve, respectively, for $\gamma'B/p'^*_{co}$ varying from 0.76 to 4.75. When $\gamma'B/p'^*_{co} \leqslant 1$, the influence of e^*_{cs} on the bearing response can be ignored. However, for $\gamma'B/p'^*_{co} > 1$, both the elastic and plastic gradients increase with increasing e^*_{cs} and the combined influence of e^*_{cs} and $\gamma'B/p'^*_{co}$ on these gradients can be expressed as:

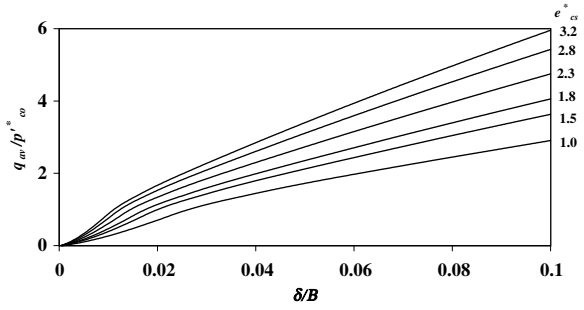

Fig. 13. Influence of e^*_{cs} on the bearing response (B = 5 m).

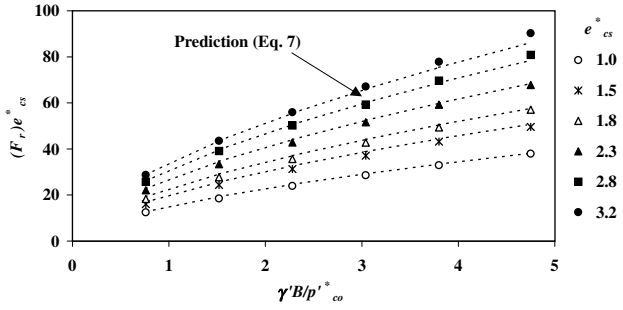

Fig. 14. Variation of elastic gradient, F_r, with e^*_{cs} and $\gamma'B/p'^*_{co}$.

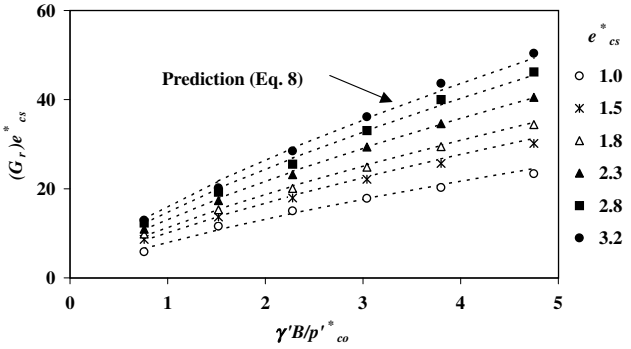

Fig. 15. Variation of plastic gradient, G_r, with e^*_{cs} and $\gamma'B/p'^*_{co}$.

$$(F_r)_{e^*_{cs}} = 15(e^*_{cs})^{0.7}\left(\frac{\gamma'B}{p'^*_{co}}\right)^{0.6} \tag{7}$$

$$(G_r)_{e^*_{cs}} = 8(e^*_{cs})^{0.6}\left(\frac{\gamma'B}{p'^*_{co}}\right)^{0.72} \tag{8}$$

5.1.6. Derivation of the bearing response curve for reconstituted soil

Eqs. (1), (2) and (4)–(8) show the influence of each critical state soil parameter on the elastic gradient, F_r, yield point, Y_r, and the plastic gradient, G_r for reconstituted (destructured) soil. Some reduction of these expressions is possible, so that ultimately only three equations are needed to represent the combined influence of the critical state parameters on F_r, Y_r and G_r, which define the complete bearing response of the reconstituted soil. Subsequently the influence of structural properties of the soil will be incorporated into these three equations to obtain expressions for F_s, Y_s and G_s, which describe the response of a structured soil.

A simple multiplicative technique has been used to derive equations for F_r, Y_r and G_r incorporating the influence of all reconstituted soil properties and $\gamma'B/p'^*_{co}$. For the elastic gradient, F_r, only κ^*, v^* and e^*_{cs} have a significant influence. Since the influence of κ^* on the bearing response was derived assuming $v^* = 0.25$ and $e^*_{cs} = 1.8$, an expression for F_r that incorporates other values of v^* and e^*_{cs} is derived assuming that the effect of each parameter is multiplicative, as follows:

$$F_r = (F_r)_{\kappa^*}\frac{(F_r)_{v^*}}{(F_r)_{v^*=0.25}}\frac{(F_r)_{e^*_{cs}}}{(F_r)_{e^*_{cs}=1.8}} \tag{9}$$

By substituting $(F_r)_{\kappa^*}$, $(F_r)_{v^*}$ and $(F_r)_{e^*_{cs}}$ from Eqs. (1), (6) and (7), respectively, the elastic gradient, F_r, can be represented in terms of $\gamma'B/p'^*_{co}$, κ^*, v^* and e^*_{cs} as shown below:

$$F_r = (\kappa^*)^{-1}(1.5 - 2.55v^*)(e^*_{cs})^{0.7}\left(\frac{\gamma'B}{p'^*_{co}}\right)^{0.6} \tag{10}$$

In the derivation of Eq. (10), it has been demonstrated that the influence of λ^* and M^* on the elastic gradient, F_r, is small enough to be ignored. The accuracy of this approach will be demonstrated later in the paper.

The yield point, Y_r, varies significantly only with M^* and $\gamma'B/p'^*_{co}$ and therefore Y_r is given by Eq. (4), which is repeated below for completeness:

$$Y_r = (Y_r)_{M^*} = (M^*)^{1.25}\left(\frac{\gamma'B}{p'^*_{co}}\right)^{m} \tag{11}$$

where $m = 0.25(M^*)^{-0.75}$.

The plastic gradient, G_r, varies significantly with three parameters λ^*, M^* and e^*_{cs}. Therefore, similar to F_r, an equation for G_r can be derived as shown below:

$$G_r = (G_r)_{\lambda^*}\frac{(G_r)_{M^*}}{(G_r)_{M^*=1.2}}\frac{(G_r)_{e^*_{cs}}}{(G_r)_{e^*_{cs}=1.8}}(0.25(\lambda^*)^{-0.6}+0.75(M^*)^{-0.6}-0.67)$$
$$= 2.0(M^*)^3(\lambda^*)^{-0.4}(e^*_{cs})^{0.6}\left(\frac{\gamma' B}{p'^*_{co}}\right) \quad (12)$$

Eqs. (10)–(12) can be used to obtain values for F_r, Y_r and G_r for a circular footing of any diameter if the intrinsic soil properties κ^*, λ^*, M^*, v^* and e^*_{cs} are known. For convenience these expressions are also summarized in Table 2.

5.2. Bearing response curve for a structured soil

In this section, the influence of soil structure on the long-term (fully drained) bearing response is studied by varying the parameters, which govern the structural features of the soil, i.e., b, Δe_i, ω and p'_{co} for different values of $\gamma' B/p'^*_{co}$.

As shown in Fig. 1, for a given structured soil, the size of the yield surface, p'_{co}, and the parameter $\Delta e_i/(\lambda^* - \kappa^*)$ are linked and their values can be related to the size of the yield surface for the same soil in a reconstituted state, p'^*_{co}, as shown below:

$$p'_{co} = p'^*_{co}\exp\left(\frac{\Delta e_i}{\lambda^* - \kappa^*}\right) \quad (13)$$

Hence, the parameter $\Delta e_i/(\lambda^* - \kappa^*)$, takes into account the combined influence of both Δe_i and p'_{co} for a particular soil and can be used to define the degree of soil structure with respect to the same soil in a reconstituted state. It is convenient to define an additional parameter, $\Delta e'_i$, as follows:

$$\Delta e'_i = \Delta e_i/(\lambda^* - \kappa^*) \quad (14)$$

The finite element analyses carried out by varying ω show that its influence on the long-term bearing capacity is not significant. Therefore, in this section, the influence of soil structure on the bearing response of a particular footing is studied by varying only the destructuring index, b, and the degree of soil structure defined by $\Delta e'_i$. The values of other parameters used for this study are the same as those given in Table 1.

5.2.1. Influence of degree of soil structure on the bearing response

Fig. 16 shows the influence of $\Delta e'_i$ on the bearing capacity for a 5 m diameter surface circular footing when b is 0.25. As $\Delta e'_i$ increases, the soil shows much stiffer response. For example, when $\Delta e'_i = \Delta e_i/(\lambda^* - \kappa^*)$ changes from 1.0 to 2.5, the bearing resistance at a footing displacement equivalent to 12% of the footing diameter shows a 3-fold increase. If soil structure is not taken into account, the predicted bearing resistance is only about half of that obtained for a structured soil for which $\Delta e'_i$ is 1.5 ($p'_{co} = 4.5p'^*_{co}$). According to Fig. 16, $\Delta e'_i$ has a significant influence only on the elastic gradient, F_s, and the yield point, Y_s, of the bearing response curve for structured soils. For different values of $\Delta e'_i$ the plastic portions of each curve are virtually parallel to each other, and so the influence of $\Delta e'_i$ on the plastic gradient can be ignored.

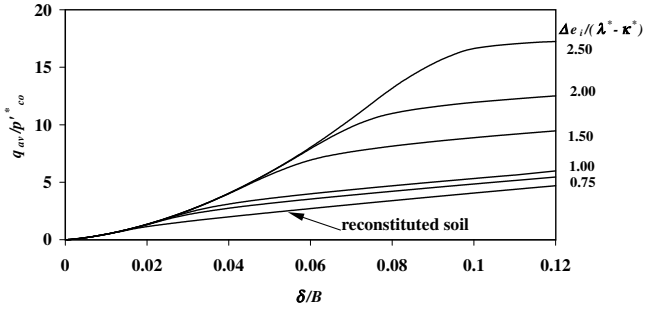

Fig. 16. Influence of $\Delta e_i/(\lambda^* - \kappa^*)$ on the bearing response (B = 5 m).

Figs. 17 and 18 show the combined influence of $\Delta e'_i$ and $\gamma' B/p'^*_{co}$ on the elastic gradient, F_s, and the yield point, Y_s. When $\Delta e'_i \leqslant 1$, the influence of soil structure on the bearing response is small and the bearing response is about 20% greater than that of the reconstituted soil. For $\Delta e'_i > 1$, the influence of soil structure on bearing resistance is significant. If the influence of soil structure is ignored for $\Delta e'_i > 1$, the error in the predicted response would be very large. Also, the influence of soil structure is more significant for larger values of $\gamma' B/p'^*_{co}$. Based on Figs. 17 and 18, the variation of the elastic gradient and yield point with $\gamma' B/p'^*_{co}$ and $\Delta e'_i$ is given by:

$$(F_s)_{\Delta e'_i} = 20\exp(0.5\Delta e'_i)\left(\frac{\gamma' B}{p'^*_{co}}\right)^{0.6} \quad (15)$$

$$(Y_s)_{\Delta e'_i} = 1.1\exp(\Delta e'_i)\left(\frac{\gamma' B}{p'^*_{co}}\right)^{0.2} \quad (16)$$

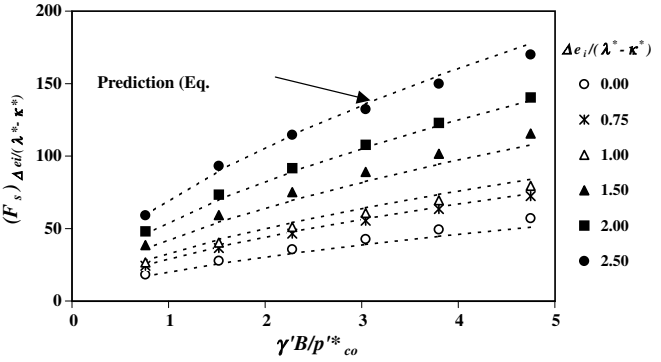

Fig. 17. Variation of elastic gradient, F_s, with $\Delta e_i/(\lambda^* - \kappa^*)$ and $\gamma' B/p'^*_{co}$.

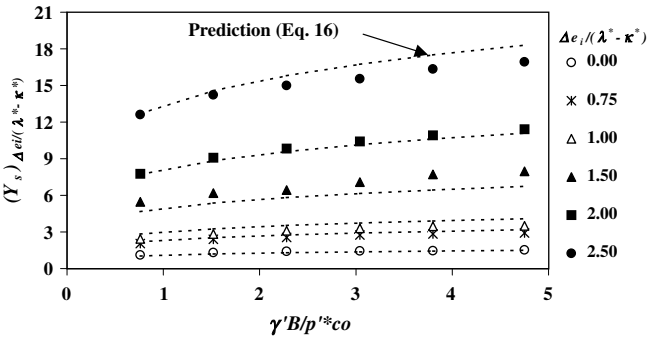

Fig. 18. Variation of yield point, Y_s, with $\Delta e_i/(\lambda^* - \kappa^*)$ and $\gamma' B/p'^*_{co}$.

Table 2
Summary of approximate expressions describing the bilinear bearing response of a rigid circular footing

Quantity	Expression
Reconstituted soil – κ^*, λ^*, M^*, v^*, e^*_{cs}	
"Elastic" gradient	$F_r = (\kappa^*)^{-1}(1.5 - 2.55v^*)(e^*_{cs})^{0.7}\left(\frac{\gamma' B}{p'^*_{co}}\right)^{0.6}$
"Yield" point	$Y_r = (M^*)^{1.25}\left(\frac{\gamma' B}{p'^*_{co}}\right)^{0.25(M^*)^{-0.75}}$
"Plastic" gradient	$G_r = 2.0(M^*)^3(\lambda^*)^{-0.4}(e^*_{cs})^{0.6}\left(\frac{\gamma' B}{p'^*_{co}}\right)^{(0.25(\lambda^*)^{-0.6}+0.75(M^*)^{-0.6}-0.67)}$
Structured soil – κ^*, λ^*, M^*, v^*, e^*_{cs}, Δe_i, b	
"Elastic" gradient	$F_s = \exp(0.5\Delta e'_i)F_r$, where $\Delta e'_i = \Delta e_i/(\lambda^* - \kappa^*)$
"Yield" point	$Y_s = \exp(\Delta e'_i)Y_r$
"Plastic" gradient	$G_s = (10b)^{-0.52\left(\frac{\gamma' B}{p'^*_{co}}\right)^{-1.17}} G_r$

5.2.2. Influence of destructuring index on bearing response

The destructuring index, b, of a structured soil defines the rate at which soil structure is lost during yielding. For soils with higher values of destructuring index, the structure is completely lost with only a small change in the stress state beyond first yield. Fig. 19 shows the influence of the destructuring index on bearing response for a 5 m diameter surface circular footing when the degree of soil structure, $\Delta e_i'$, is 1.5. It can be seen that b has an influence on the bearing capacity only beyond the yield point where the soil behaviour is predominantly plastic.

Fig. 20 shows the variation of plastic gradient with the logarithm of b for a range values of $\gamma' B/p_{co}'^{*}$. For all values of $\gamma' B/p_{co}'^{*}$, the plastic gradient reduces with increasing b and the change in plastic gradient with b is significant only when $b \leqslant 4$. The finite element predictions given in Fig. 20 can be fitted quite well to the following equation:

$$(G_s)_b = \left[6.68\frac{\gamma' B}{p_{co}'^{*}} - 3.14\right] b^{-0.518\left(\gamma' B/p_{co}'^{*}\right)^{-1.17}} \tag{17}$$

5.2.3. Derivation of bearing response curve for structured soil

In Section 5.1.6 a method was suggested to obtain the bearing response curve for any reconstituted soil based on the intrinsic soil parameters, neglecting the influence of soil structure. In this section expressions derived for a reconstituted soil are modified by incorporating the influence of soil structure.

According to the results presented in Section 5.2.1, only the degree of soil structure has an influence on the elastic gradient and the yield point. When $\Delta e_i'$ is zero, soil does not have any structure and behaves similar to the same material at the reconstituted state. Therefore, the influence of degree of soil structure on the elastic gradient and the yield point can be described to sufficient accuracy by:

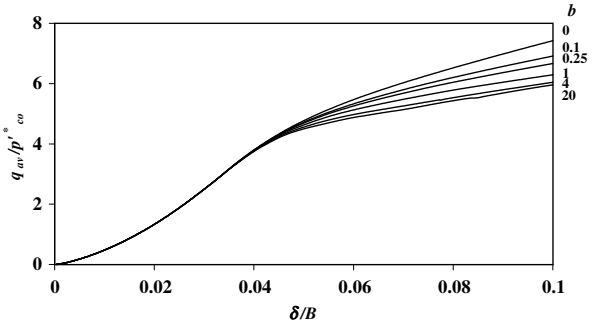

Fig. 19. Influence of destructuring index, b, on the bearing response (B = 5 m).

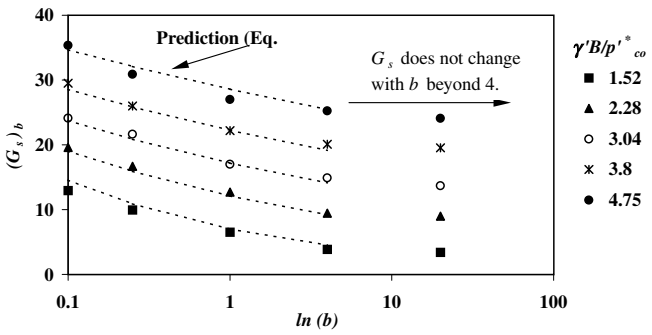

Fig. 20. Variation of plastic gradient, G_s, with destructuring index, b, and $\gamma' B/p_{co}'^{*}$.

$$\frac{F_s}{F_r} = \frac{(F_s)_{\Delta e_i'}}{(F_s)_{\Delta e_i'=0}} = \exp(0.5\Delta e_i') \tag{18}$$

$$\frac{Y_s}{Y_r} = \frac{(Y_s)_{\Delta e_i'}}{(Y_s)_{\Delta e_i'=0}} = \exp(\Delta e_i') \tag{19}$$

The plastic gradient of the bearing response curve is influenced significantly only by the destructuring index, b. For any value of b, the plastic gradients are nearly the same for all values of $\Delta e_i' = \Delta e_i/(\lambda^* - \kappa^*)$. However, when b is 0.1, plastic gradient, G_s, of a structured soil and plastic gradient for the reconstituted soil of the same material, G_r, are nearly the same. Hence, the influence of b on plastic gradient of the bearing response curve for a structured soil can be represented by:

$$\frac{G_s}{G_r} = \frac{(G_s)_b}{(G_s)_{b=0.1}} = (10b)^{-0.52\left(\gamma' B/p_{co}'^{*}\right)^{-1.17}} \tag{20}$$

When applying this method, first F_r, Y_r and G_r have to be calculated using Eqs. (10)–(12), respectively, based on the intrinsic properties of the reconstituted soil. If $\Delta e_i' \leqslant 1$, the influence of degree of soil structure on bearing capacity can be ignored. If $\Delta e_i' > 1$, Eqs. (18) and (19) can be used to compute F_s and Y_s. Finally Eq. (20) can be used to incorporate the influence of the destructuring index, b, on the plastic gradient of the bearing response curve, G_s. For convenience, these relationships are summarised in Table 2.

6. Validation of the new method

In order to validate the proposed procedure, results predicted for different $\Delta e_i'$ and b using Eqs. (10), (11), (12), (18), (19) and (20) are compared with the results obtained from the finite element analyses. According to the results given in Table 3, it is clear that the error in predicted values are less than 10%, which is generally acceptable for foundation design purposes. Although results are given in Table 3 for some selected cases, the proposed method has shown reasonable agreement with the finite element analyses for different soil conditions and foundation sizes.

Next the capability of the proposed method for predicting the long-term or drained bearing response of surface circular footings have been demonstrated using the plate load tests carried out by Consoli et al. [3]. These tests were carried out in homogeneous lightly cemented residual soils in Southern Brazil. The upper surface soil at this site consisted of 4 m of lightly cemented homoge-

Table 3
Comparison of finite element results with the proposed equations

$\gamma' B/p_{co}'^{*}$	$\Delta e_i' = 2.5$, $b = 0.25$					
	F_s		Y_s		G_s	
	FEM	Eq. (18)	FEM	Eq. (19)	FEM	Eq. (20)
1.52	89.74	93.3	14.6	14.7	10.5	10.0
2.28	114.46	119.0	15.0	16.1	15.9	16.7
3.04	132.4	141.5	15.54	17.2	20.7	21.7
3.8	150.0	161.8	16.34	18.0	25.4	26.0
4.75	170.1	184.0	16.94	18.9	30.5	31.1
$\gamma' B/p_{co}'^{*}$	$\Delta e_i' = 1.5$, $b = 4$					
	F_s		Y_s		G_s	
	FEM	Eq. (18)	FEM	Eq. (19)	FEM	Eq. (20)
1.52	59.25	59.5	6.18	5.72	4.51	4.3
2.28	75.05	75.9	6.43	6.25	9.19	9.16
3.04	89.02	90.2	7.08	6.7	14.9	14.0
3.8	101.62	103.1	7.72	7.0	20.1	19.0
4.75	115.59	117.9	7.97	7.3	25.46	24.3

neous sandy silty red clay. Below that there was a 2 m thick layer of highly cemented red silty clay. The tests were carried out using rigid circular steel plates to load the soil at a depth of 1.2 m below the ground level. There were no embedment effects on the footing response because the upper 1.2 m of soil was removed over a large area of the test site.

Circular plate load tests carried out for 45 cm and 60 cm diameter plates have been simulated using the finite element method and the approximate method described previously. The values of soil parameters used to simulate these tests are given in Table 4. These values were obtained by simulating the drained triaxial test results given for the samples of residual soil. Fig. 21 shows the drained triaxial test results and numerical simulations using the Structured Cam Clay model.

Table 4
Properties for cemented residual soil assumed for the plate load test site

Symbol	Property	Value
λ^*	Gradient of the normal compression line in $e - \ln(p')$ space	0.22
κ^*	Gradient of the unloading and reloading line in $e - \ln(p')$ space	0.002
M^*	Aspect ratio for the yield surface	1.72
ν^*	Poisson's ratio	0.4
b	Destructuring index	0.08
Δe_i	Additional voids ratio sustained by soil structure	0.5
e^*_{cs}	Void ratio at the $p' = 1$ on the CSL in $e - \ln(p')$ space	3.2
p'_{co}	Size of the initial (structural) yield surface at ground surface	150 kPa
dp'_{co}/dz	Gradient of p'_{co} with depth below the ground surface	10 kPa/m
ω	parameter defining the plastic potential	1
K_o	Coefficient of earth pressure at rest	0.6
γ	bulk unit weight of soil (water table assumed at ground surface)	20 kN/m^3

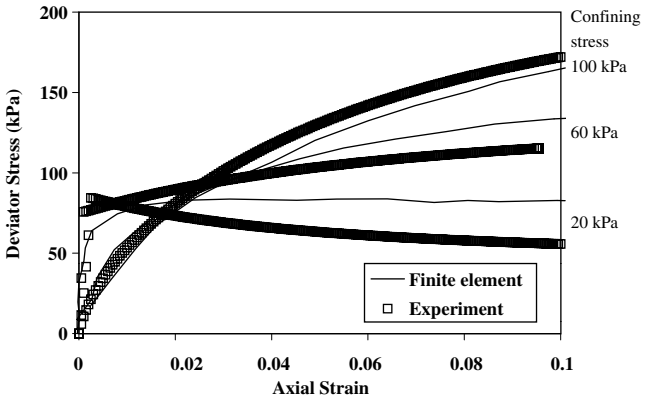

Fig. 21. Comparison of experimental and finite element results for triaxial tests.

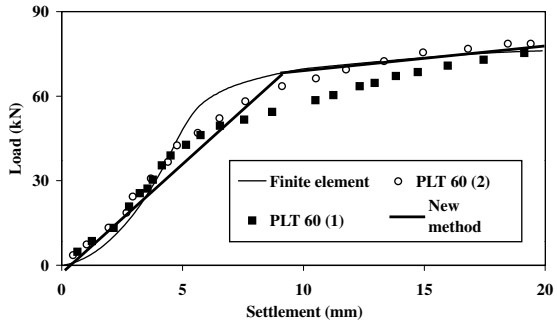

Fig. 22. Predicted bearing response using the new method for 60 cm diameter footing.

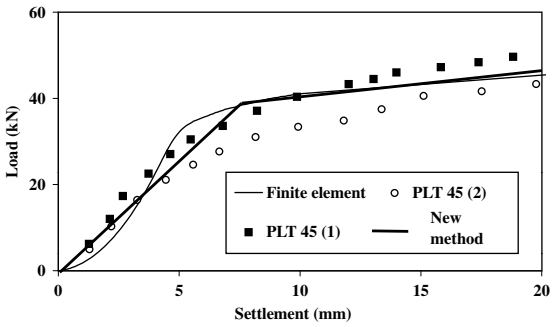

Fig. 23. Predicted bearing response using the new method for 45 cm diameter footing.

Figs. 22 and 23 show, respectively, the plate load tests for 60 cm and 45 cm rigid steel plates. When using the new method, firstly the gradients and the yield pressure are calculated assuming reconstituted soil properties. Next, based on the degree of soil structure and the destructuring index, the gradients and the yield pressure for the structured soil can be obtained. Finally, these values can be used to obtain the bearing response of the circular footing on the structured soil.

According to the parameter values given in Table 4, the degree of soil structure, $\Delta e'_i = \Delta e_i/(\lambda^* - \kappa^*)$, for the cemented soil is 2.3. Since $\Delta e'_i > 1$, the influence of degree of soil structure on the bearing response is significant and it should be incorporated into the values calculated for F_s and Y_s. Also, the influence of the destructuring index, b, has to be incorporated into the value selected for G_s.

Eqs. (10)–(12) can be used to obtain F_r, Y_r and G_r, respectively. For cemented soil, when $B = 0.45$ m, it is found that $F_r = 260$, $Y_r = 1.6$ and $G_r = 20$, and when $B = 0.6$ m, $F_r = 310$, $Y_r = 1.7$ and $G_r = 20$. Next, based on the structural properties of the soil, F_s/F_r, Y_s/Y_r and G_s/G_r can be obtained from Eqs. (18)–(20), respectively. These ratios are independent of footing size. Therefore, for $B = 0.45$ m and $B = 0.6$ m, $F_s/F_r = 3.1$, $Y_s/Y_r = 9.9$ and $G_s/G_r = 1.8$. Figs. 22 and 23 show the bearing response obtained for the footings using the new approximate method. Only displacements up to 20 mm have been plotted in order to see more closely the level of agreement between elastic gradients obtained from the new method, finite element results and the field tests. Although the simplified method is derived based on the finite element results, there is a discrepancy between the elastic gradients obtained from the finite element method and the simplified method due to the shape of the initially assumed bilinear distribution (Fig. 3a). Also the finite element results show more soil compressibility during the initial loading phase than that observed during the plate load test. Nevertheless, there is a reasonable agreement between the bilinear approximation predicted for the structured soil from the new method and the bearing pressure curve obtained from the plate load test, which is sufficient for practical purposes.

7. Conclusions

The influence of soil structure on the bearing response of circular footings has been investigated using the Structured Cam Clay model. It was found that under fully drained conditions, deformation of the soil beneath the footing occurs as a punching or local shear failure. A parametric study has been carried out by varying the parameters which characterize the structural features of the soil. A novel method has been presented to obtain the relationship between the bearing pressure and footing displacement for a circular footing resting on a structured soil deposit. Application of the new method has been demonstrated using field plate load tests carried out on cemented residual soil in Southern Brazil.

The bilinear bearing pressure curves predicted using the new method show reasonable agreement with the field plate load tests and finite element simulations. This suggests that the approximate method presented in this paper could be quite useful for predicting the bearing response of footings on structured soil.

References

[1] Carter JP, Balaam NP. AFENA user manual, Version 6. Centre for Geotechnical Research. University of Sydney; 1995.

[2] Carter JP, Booker JR, Yeung SK. Cavity expansion in cohesive frictional soils. Géotechnique 1986;36:349–58.

[3] Consoli NC, Achnaid F, Milititsky J. Interpretation of plate load tests on residual soil site. J Geotech Geoenviron Eng, ASCE 1998;124(9):857–67.

[4] Gens A, Nova R. Conceptual bases for a constitutive model for bonded soils and weak rocks. In: Proceedings of the international symposium on geotechnical engineering of hard soils – soft rocks; 1993. p. 485–94.

[5] Islam K. Constitutive models for carbonate sands and their application to footing problems. PhD thesis, Centre for Geotechnical Research, University of Sydney, Australia; 1999.

[6] King R, Lodge M. North west shelf development – the foundation engineering challenge. In: Proceedings of the international conference on calcareous sediments, vol. 2; 1988. p. 333–42.

[7] Ladanyi B. Expansion of cavities in a brittle media. Int J Rock Mech Min Sci 1967;4:301–28.

[8] Leroueil S, Vaughan PR. The general and congruent effects of structure in natural soils and weak rocks. Géotechnique 1999;40(3):467–88.

[9] Liu MD, Carter JP. A Structured Cam Clay model. Can Geotech J 2002;39(6):1313–32.

[10] Liyanapathirana DS, Carter JP, Airey DW. Non-homogeneous behaviour of structured soils during triaxial testing. Int J Geomech 2005;5(1):10–23.

[11] Potts DM, Jones ME, Berget OP. Subsidence above the Ekofisk oil reservoirs. In: Proceedings of the 5th international conference on the behaviour of offshore structures, Trondheim, vol. 1; 1988. p. 113–27.

[12] Poulos HG, Chua EW. Bearing capacity of foundation on calcareous sand. In: Proceedings of 11th ICSMFE, vol. 3; 1985. p. 1619–22.

[13] Poulos HG, Chua EW, Hull TS. Settlement of model footings on calcareous sand. Geotech Eng 1984;15:21–35.

[14] Roscoe KH, Burland JB. On the generalised stress–strain behaviour of wet clay. In: Heyman J, Leckie FA, editors. Engineering plasticity. Cambridge: Cambridge University Press; 1968. p. 535–609.

[15] Rouainia M, Muir Wood D. A kinematic hardening model for natural clays with loss of structure. Géotechnique 2000;50(2):153–64.

[16] Sharp DE, Seters AJ. Results and evaluation of plate load test results. In: Proceedings of the international conference on calcareous sediments, Perth, Australia; 1998. p. 473–83.

[17] Terzaghi K. Theoretical soil mechanics. New York: John Wiley and Sons Inc; 1943.

[18] Vesic AS. Expansion of cavities in infinite soil mass. J Soil Mech Found Div, ASCE 1972;98(SM3):265–90.

[19] Whittle AJ. Evaluation of a constitutive model for overconsolidated clays. Géotechnique 1993;43(2):289–314.

[20] Woodward PK, Nesnas K, Griffiths DV. Advanced numerical modeling of footings on granular soils. Geotechnical Special Publication No. 96; 2000. p. 88–101.

[21] Yeoh CK. Cyclic response of an artificially cemented soil and foundations. PhD thesis, University of Sydney; 1996.